Journal of Materials Chemistry A

Accepted Manuscript

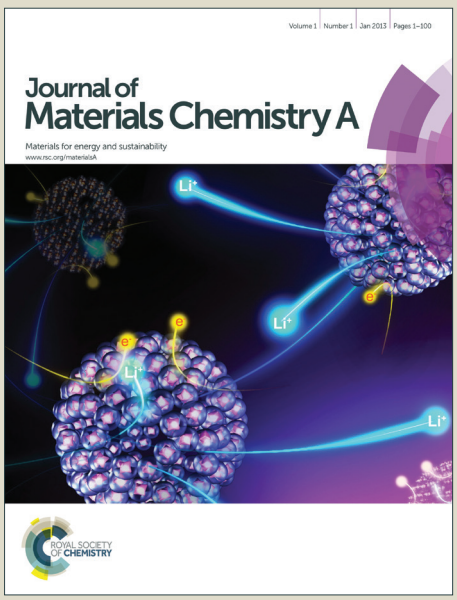

ROYAL SOCIETY OF CHEMISTRY

www.rsc.org/materialsA

Journal of Materials Chemistry A

Cite this: DOI: 10.1039/c0xx00000x

PAPER

www.rsc.org/xxxxxx

Surface Modification of TiO_2 Nanotube Arrays with Y_2O_3 Barrier Layer: Controlling Charge Recombination Dynamics in Dye-sensitized Solar Cells

Lu–Yin Lin,[a,b] Min–Hsin Yeh,[a] Chia–Yuan Chen,[b] R. Vittal,[a] Chun–Guey Wu[b*] and Kuo–Chuan Ho[a,c]**

Received (in XXX, XXX) Xth XXXXXXXXX 20XX, Accepted Xth XXXXXXXXX 20XX
DOI: 10.1039/b000000x

Fast electron transport, large specific surface area, and slow interfacial electron recombination are indispensable features for an efficient photoelectrode of dye–sensitized solar cells (DSSCs). Highly–ordered TiO_2 nanotubes (TNT) with advanced architecture of high surface–to–volume ratio and open–up geometry for providing direct electrons/ions transport channels is applied on a flexible photoanode in this study. Due to several micrometers in the semiconductor are required for diffusion of electrons, which are surrounded by electron acceptors at a distance of only several nanometers, a wide band gap barrier layer of Y_2O_3 is coated on TNT to retard back transfer of electrons to the electrolyte or to the oxidized dye molecules, by electrodepositing $Y(OH)_3$ on TNT surfaces and subsequently annealing the samples. By adjusting the charge capacity for $Y(OH)_3$ electrodeposition, the charge recombination dynamics in the pertinent DSSC can be easily controlled. This barrier layer also enhances the dye adsorption and therefore increases the volume of optically active component due to the more basic surface of Y_2O_3 for more carboxyl groups in a dye molecule adsorbing onto the surface. A higher light–to–power conversion efficiency (η) of 6.52% is obtained for the pertinent DSSC, with compared to a reference cell with non–coated TNT (η = 5.35%), exhibiting a 22% enhancement on the η.

Introduction

Dye–sensitized solar cells (DSSCs) have been researched extensively since their first innovative report in 1991.[1] The challenging issues lie not only on achieving high light–to–power conversion efficiency (η) but also on pursuing easy and low–cost manufacturing techniques. Flexible DSSCs with the photoanode composed of one–dimensional (1–D) TiO_2 nanotubes (TNT) have attracted much attention since the possibility of roll–to–roll production and the features of high surface–to–volume ratio and open–up geometry for TNT to provide higher dye loading amount and direct electrons/ions transport channels.[2-5] Nakayama *et al.* applied TNT as an underlayer in the photoanode to raise the light harvesting efficiency of DSSCs.[6] Xu *et al.* prepared a bilayered film with TiO_2 nanoparticles (TNP) and TNT respectively as the underlayer and the overlayer on the photoanode to realize rapid electron transfer.[7] We have previously prepared a flexible photoanode with TNT as the underlayer and TNP as the overlayer on Ti foils to produce 1–D electron transfer paths at the interface between the Ti foil and TNP.[8] To further improve electron transfer and minimize electron–hole recombination, surface modification of TiO_2 with other metal oxides, *e.g.*, SrO,[9] Nb_2O_3,[10] $SrTiO_3$,[11] ZnO,[12] and MgO[13], have been studied for several years.[9-19] The coated metal oxides allows the photo–injected electrons to tunnel through into TiO_2 core, and subsequently to the conducting oxide layer of the substrate. Simultaneously, the coated metal oxides form an energy barrier for the recombination reactions of the injected electrons from the TiO_2 core to triiodide ions in the electrolyte and also to the oxidized dye molecules. This process is energetically favourable only if the conduction band of the coated metal oxides lies above both the lowest unoccupied molecular orbital (LUMO) energy level of the sensitizer and the conduction band edge of the TiO_2 core.[16] In addition, the surface of the metal oxide coating is often more basic, leading to higher adsorption of carboxyl groups in dye molecules and therefore to higher volume of optically active components. Guillén *et al.* developed a multistep wet–chemistry route to obtain ZnO nanowires arrays coated by a ZnO nanocrystalline layer. Decreased recombination rate and improved photovoltage are obtained for the pertinent cells.[20] Gao *et al.* fabricated SnO_2/TiO_2 core–shell DSSCs to obtain fast and efficient charge collection. A η of 5.11% was obtained for the core–shell DSSCs, which is above five times higher than that of the SnO_2 nanotube based DSSCs (η = 0.99%).[21] Chen *et al.* fabricated a TNT film filled with TNP coated by a thin SrO layer and got a η of 5.39% for the pertinent DSSC.[22] Lee *et al.* prepared porous TiO_2 films coated with ZrO_2 or Nb_2O_5 thin layers and found reduced charge injection and back electron transfer rates for the pertinent DSSCs with compared to those of

the cell with a bare TiO_2 film.[23] In this study, flexible photoanodes were prepared by anodizing Ti foils to obtain TNT on the surfaces. The TNT length was optimized in considering of the electron transport and the specific surface area for dye adsorption. It is well-known that the insulating yttrium oxide (Y_2O_3) has attractive features including high-κ dielectrical value, a wide bandgap energy of 6 eV, a relatively high dielectric constant, high thermal stability, and low leakage current.[24-26] Therefore, to further reduce the interfacial electron recombination, $Y(OH)_3$ was electrodeposited on TNT and the resulting film was annealed subsequently to obtain a thin Y_2O_3 barrier layer on the surface of TNT. The charge recombination dynamics in the pertinent DSSC can be easily controlled via adjusting the charge capacity for $Y(OH)_3$ electrodeposition. In addition, the more basic surface of Y_2O_3 is favour for the carboxyl groups in a sensitizer adsorbing to increase the dye adsorption. A better η of 6.52% was achieved for the DSSC with Y_2O_3–coated TNT (Y–TNT) on a Ti foil as the photoanode, with reference to that of a cell with TNT (5.35%). The Y–TNT film was characterized by scanning electron microscopy (SEM), X–ray diffraction (XRD), and X–ray photoelectron spectroscopy (XPS). Electrochemical impedance spectra (EIS), incident photon to current conversion efficiency (IPCE) curves, and laser–induced photo–potential transients were utilized to substantiate the explanations.

Experimental Section

Materials

Lithium iodide (LiI, synthetical grade) and iodine (I_2, synthetical grade) were obtained from Merck. Tert–butyl alcohol (tBA, 96%) and 4–tert–butylpyridine (TBP, 96%) were obtained from Acros. Neutral cleaner, isopropyl alcohol (IPA, 99.5%) and yttrium nitride ($Y(NO_3)_3 \cdot 6H_2O$) were obtained from Aldrich. 3–methoxypropionitrile (MPN, 99%) was obtained from Fluka. Acetonitrile (ACN, 99.99%) and ammonium fluoride (NH_4F, A. C. S. reagent) were obtained from J. T. Baker. Ethylene glycol (EG, extra pure) was obtained from Scharlau. 1–Propyl–2,3–dimethylimidazolium iodide (DMPII) was obtained from Solaronix. The organic solvent electrolyte contains a mixture of 0.1 M LiI, 0.6 M DMPII, 0.05 M I_2, and 0.5 M TBP in a solvent of 50 vol% MPN and 50 vol% ACN.

Preparation of photoanode/Pt counter electrode and cell assembly

Ti foils (0.4 mm thick, 99.8% purity, Fuu Cherng Co. Ltd., Taiwan) were polished to remove residual metal oxides and other adhesive substances, and sequentially cleaned with a neutral cleaner, deionized–water (DI–water), acetone, and IPA. Highly ordered TNT was prepared on Ti foils using an anodization method.[8, 27, 28] The anodization process was conducted at a constant applied potential of 50 V at the room temperature in an electrolyte consisting of 0.25 wt% NH_4F and 1.0 wt% H_2O in ethylene glycol (EG). The anodized sample sheet was ultrasonically cleaned in DI–water for 1 min to remove the surface debris. $Y(OH)_3$ was then electrodeposited on TNT using a conventional three electrode cell in a 0.01 M $Y(NO_3)_3$ solution at the deposition charge capacities of 10, 15, 20, and 25 mC cm^{-2}. (Equation (1)) The potential of the working electrode was fixed at –1.2 V *vs.* the Ag/AgCl reference electrode. The TNT film without the electrodeposition of $Y(OH)_3$ was used for the comparative purpose. The TNT films with and without $Y(OH)_3$ electrodeposition were gradually heated to a temperature of 500 °C in an oxygen atmosphere, and subsequently annealed at this temperature for 1 h. The $Y(OH)_3$ layer coated on TNT was then changed to a Y_2O_3 thin layer after annealing (Equation (2)).

$$Y(NO_3)_3 + 3\ H_2O \rightarrow Y(OH)_3 + 3\ HNO_3 \quad (1)$$

$$4\ Y(OH)_3 + 3\ O_2 \rightarrow 2\ Y_2O_3 + 12\ OH^- \quad (2)$$

After annealing and cooling to the room temperature, a portion (0.4×0.4 cm^2) of the resulting films was selected as the active area by removing the side portions carefully, and following the films were immersed in a 0.3 mM solution of TBA (Ru[(4–carboxylic acid–4'–carboxylate–2,2'–bipyridine)(Ligand–11)$(NCS)_2$])) (CY C–B11)[29] in a solvent mixture of ACN and tBA (volume ratio of 1:1), at room temperature for 24 h; 20 mM chenodeoxycholic acid (CDCA, ≥ 95%) was used as a co–adsorbent along with the dye. The dye–sensitized TiO_2 electrode was then coupled with a transparent Pt counter electrode. The counter electrode was prepared by sputtering Pt on an ITO glass (ITO, UR–ITO007–0.7mm, Uni–onward Corp., Taiwan, < 7 Ω $sq.^{-1}$) which was first cleaned with a neutral cleaner, and then washed with DI–water, acetone, and IPA, sequentially; the sputtering was carried out for 5 s (under a sputter current of 40 mA), which was the optimized condition according to our previous study,[30] in consideration of the catalytic ability of Pt and its transmittance for a back–illuminated DSSC. The two electrodes were separated by a 60 μm thick gasket made of ionomer Surlyn (SX1170–25, Solaronix S.A., Aubonne, Switzerland) and sealed by heating. The electrolyte was injected into the gap between the electrodes by capillarity.

Measurements

The DSSCs were illuminated by a class A quality solar simulator (XES–301S, AM1.5G, San–Ei Electric Co., Ltd., Osaka, Japan) from the side of Pt/ITO (back–illumination) and the incident light intensity (100 mW cm^{-2}) was calibrated with a standard Si cell (PECSI01, Peccell Technologies, Inc.). The photoelectrochemical characteristics of the DSSCs were recorded with a potentiostat/galvanostat (PGSTAT 30, Autolab, Eco–Chemie, the Netherlands). The crystalline phase and the chemical bonding state of the films of TNT and Y–TNT were studied by X–ray diffraction (XRD, MO3XHF, MAC) and X–ray photoelectron spectroscopy (XPS, Theta Probe, Thermo Fisher Scientific, UK), respectively. Surface morphologies of TNT films were observed by scanning electron microscopy (SEM, Nova NanoSEM 230, FEI). Electrochemical impedance spectra (EIS) were obtained by the above–mentioned potentiostat/galvanostat equipped with an FRA2 module, under a constant light illumination of 100 mW cm^{-2}. The frequency range explored was 10 mHz to 65 kHz. The applied bias potential was set at the open–circuit potential of the DSSC, between the Pt counter electrode and the photoanode, starting from the short–circuit condition; the corresponding ac amplitude was 10 mV. The impedance spectra were analyzed using an equivalent circuit model.[31,32] Pulsed laser excitation was applied by a frequency–doubled Q–switched Nd:YAG laser (model Quanta–Ray GCR–3–10, Spectra–Physics laser) with a 2 Hz repetition rate at 532 nm, and a 7 ns pulse width at half–height. The average electron lifetime could approximately be estimated by fitting a decay of the open–circuit potential transient with exp ($-t\ \tau_e^{-1}$), where t is the time and τ_e is an average time

constant before recombination. Incident photo–to–current conversion efficiency (IPCE) curves were obtained at short–circuit condition. The light source was a class A quality solar simulator (PEC–L11, AM1.5G, Peccell Technologies, Inc.); light was focused through a monochromator (Oriel Instrument, model 74100) onto the photovoltaic cell. The monochromator was moved in steps through the visible spectrum to generate the IPCE (λ) as defined in Equation (3) as following,

$$\mathrm{IPCE}\ (\lambda) = 1240\left(\frac{J_{SC}}{\lambda\varphi}\right) \quad (3)$$

where λ is the wavelength, J_{SC} is the short–circuit photocurrent (mA cm^{-2}) recorded with a potentiostat/galvanostat, and φ is the incident radiative flux (W m^{-2}) measured with an optical detector (Oriel Instrument, model 71580) and a power meter (Oriel Instrument, model 70310).

Results and Discussion

Characteristics of yttrium oxide modified TiO_2 nanotube arrays

Prior to deposit yttrium oxides on the TNT electrode, the performance of the DSSCs with bare TNT photoanodes was optimized by varying the anodization time for growing TNTs. The optimization results are described in the electronic supporting information (ESI). The best performance of the TNT–based DSSCs was obtained with 50 V and 240 min as the anodization voltage and period, respectively. Hence for the following works the TNT was prepared with this best condition.

In order to further reduce the interfacial electron recombination, a post–treatment was performed with a thin barrier layer of Y_2O_3 coated on TNT. **Figure 1(a)**, **(b)**, **(c)**, and **(d)** show the SEM images of Y–TNT with the charge capacities of 10, 15, 20, and 25 mC cm^{-2}, respectively. The wall thickness of the TNT slightly increases with increasing charge capacity for electrodepositing $Y(OH)_3$ before annealing, indicating the formation of Y_2O_3 thin film on TNT. The wall thickness of Y–TNT with the charge capacity of 10, 15, 20, and 25 mC cm^{-2} were respectively estimated to be 27, 37, 43, and 50 nm, which are larger than that of the TNT, *i.e.*, 20 nm, as shown in the ESI. Furthermore, the crystalline phases of the TNT and Y–TNT films were examined by XRD patterns, as shown in **Figure 2**. Peaks corresponding to (101), (103), (004), (200), (105), (211), and (118) of the TiO_2 structure associated with the anatase phase are observed in this figure for all the XRD patterns, [33,34] indicating the TNT and Y–TNT are crystallized in pure anatase phase. The peaks of Ti foil substrate also present in this figure. However, no obvious peaks were found for Y_2O_3 in the case of Y–TNT. It is presumed that the Y_2O_3 film is too thin to be detected. Therefore, EDX was applied to further investigate the composition of Y–TNT. **Figure 3(a)** and **(b)** illustrate the EDX data of Y–TNT and TNT, respectively. Ti and O peaks were found in both **Figure 3(a)** and **(b)**, while Y peak was only observed in **Figure 3(a)**, indicating the existence of yttrium element on TNT in the case of Y–TNT. In addition, the formation of Y_2O_3 was verified by XPS. The Y 3d and Ti 2p core–level XPS spectra of Y–TNT annealed at 500 °C are shown in **Figure 4(a)** and **(b)**, respectively. Oxide Y 3d peaks located around 161 and 159 eV respectively for Y $3d_{3/2}$ and $3d_{5/2}$ characterized for Y_2O_3 were found in **Figure 4(a)**, while TiO_2 features at 458.9 eV for Ti $2p_{3/2}$ and at 464.5 eV for Ti $2p_{1/2}$ in **Figure 4(b)** reveal the presence of TiO_2 in Y–TNT.[35]

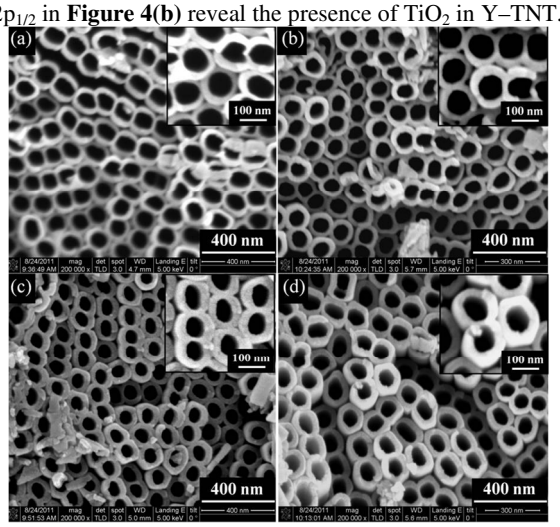

Figure 1 SEM images of Y–TNT obtained with the charge capacities of 10, 15, 20, and 25 mC cm^{-2}.

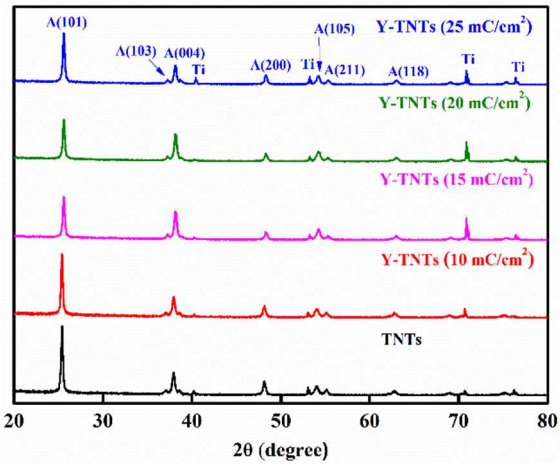

Figure 2 XRD patterns of the TNT and Y–TNT obtained with the charge capacities of 10, 15, 20, and 25 mC cm^{-2}.

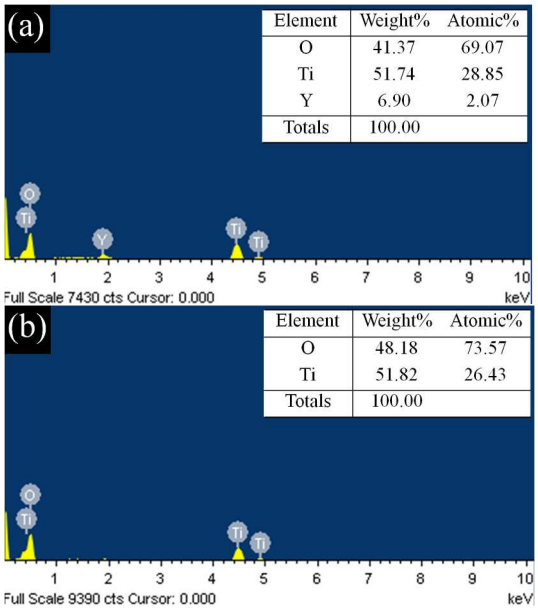

Figure 3 EDX data of (a) Y–TNT and (b) TNT.

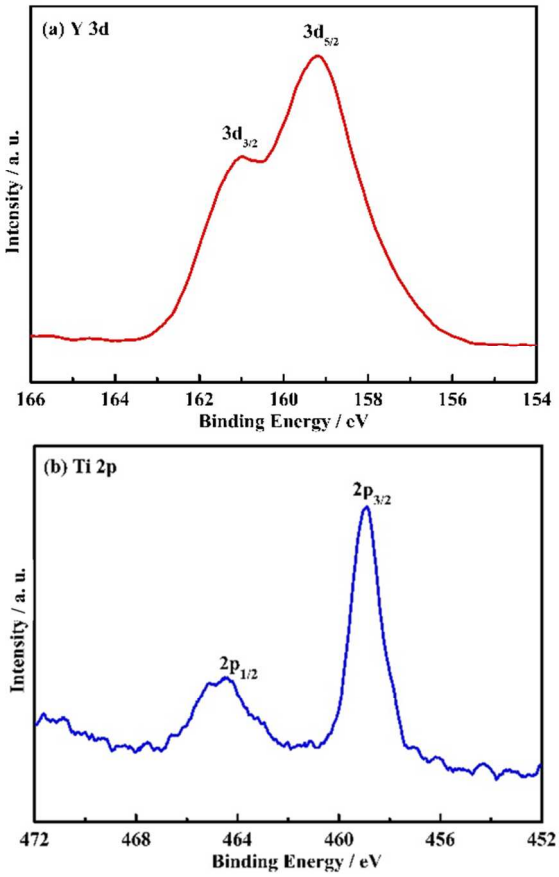

Figure 4 XPS spectra of (a) Y 3d and (b) Ti 2p for the Y–TNT.

Photovoltaic performance and incident photon–to–electron conversion efficiency of dye-sensitized solar cells with Y_2O_3 modified TiO_2 nanotube arrays

Figure 5 shows *J*–V curves of the DSSCs with TNT and Y–TNT obtained with the charge capacity of 10, 15, 20, and 25 mC cm^{-2}, and the corresponding photovoltaic parameters are summarized in **Table 1**. All the DSSCs with Y–TNTs show higher V_{OC}, compared that of the cell with TNT. These increases in *V*oc are due to energy barrier at the interface between Y–TNT and the electrolyte or the oxidized sensitizer enabled by the presence of Y_2O_3, which has a higher conduction band edge by about 3.2 V, *i.e.*, the conduction band edges of TiO_2 and Y_2O_3 are –0.20 V and –2.58 V *vs.* normal hydrogen electrode (NHE)[36-39] respectively, as shown in **Scheme 1**. This energy barrier reduces the back electron transfer from the conduction band of TiO_2 to triiodide ions or oxidized sensitizers. Also, with the increase in charge capacity for the deposition of $Y(OH)_3$, *i.e.*, with the increase of Y_2O_3 amount on TNT, the V_{OC} increases considerably, indicating the more efficient reduction for the back electron transfer with thicker Y_2O_3 layers.[11] It is also successfully confirmed that by simply adjusting the charge capacity for $Y(OH)_3$ electrodeposition on TNT, the charge recombination dynamics can be easily controlled. On the other hand, the J_{SC} increases with the increase in charge capacity up to 15 mC cm^{-2}, and decreases with further increases in charge basic than TiO_2, *i.e.*, the pzc are pH 9 and pH 6.2 for Y_2O_3 and capacity. It was reported by Kay and Grätzel that Y_2O_3 is more TiO_2, respectively.[11] The surface of Y–TNT should be more basic than

Table 1 Photovoltaic parameters of the DSSCs with bare TNT and Y–TNT obtained with the charge capacities of 10, 15, 20, and 25 mC cm^{-2}, measured at 100 mW cm^{-2}.

Deposited charge capacity /mC cm^{-2}	V_{OC} /V	J_{SC} /mA cm^{-2}	*FF*	η (%)
0	0.64	15.31	0.55	5.35
10	0.65	16.50	0.55	6.27
15	0.67	17.06	0.67	6.52
20	0.69	13.94	0.60	5.22
25	0.70	12.31	0.58	4.89

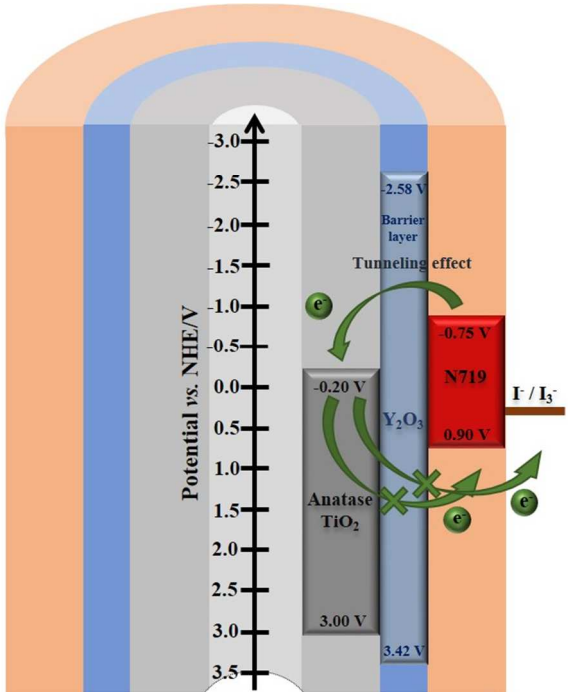

Scheme 1 Schematic diagram of the energy levels of a core–shell structure on the photoelectrode in DSSCs.

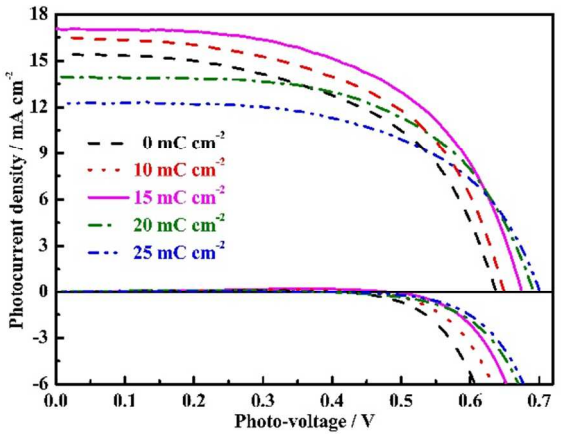

Figure 5 Current–voltage curves of the DSSCs with bare TNT and Y–TNT obtained with the charge capacities of 10, 15, 20, and 25 mC cm^{-2}, measured at 100 mW cm^{-2} and in the dark.

that of the individual structure of TiO_2, so more acidic dye molecules can adsorb on the surface, leading to higher J_{SC}.[14] However, the J_{SC} decreases with further increases in the charge capacity for $Y(OH)_3$ electrodeposition, *i.e.*, 20 and 25 mC cm^{-2}. This may be ascribed to the serious tunnelling barrier in the case of thick Y_2O_3 layers, which would inhibit the electron

transferring from dye to TiO_2. The best η of 6.52% was achieved for the DSSC with Y–TNT obtained with a charge capacity of 15 mC cm^{-2}, while the cell with TNT shows an η of only 5.35%. **Figure 5** also illustrates the current density–voltage curves of the DSSCs with TNT and Y–TNT obtained with the charge capacities of 10, 15, 20, and 25 mC cm^{-2} measured in dark. The onsets of the dark current densities for the DSSCs with Y–TNT obtained with the charge capacities of 10, 15, 20, and 25 mC cm^{-2} occur at 0.56, 0.59, 0.60, 0.61, and 0.54 V, respectively. These values were obtained by drawing tangent lines to the curves, starting from the potential scale, and a zero current line to the same curves, and by measuring the potentials that correspond to the intersection points of the tangent lines with the zero current–line. The onset of the dark current for the DSSC with TNT occurs at the lowest forward bias, indicating the most serious charge recombination in this case, while the forward bias for the onset of the dark current of the DSSCs with Y–TNT increases with increasing charge capacity, confirming again that the charge recombination can be reduced with more Y_2O_3 deposition. All the onset potentials of the cells measured in dark are in consistency with their V_{OC} values.

Figure 6 shows IPCE curves of the DSSCs with TNT and Y–TNT obtained with the charge capacities of 10, 15, 20, and 25 mC cm^{-2}. The maximum efficiency at the wavelength of 580 nm is in coincidence with the absorption maximum wavelength of CYC–B11 dye. The IPCE for the DSSC with Y–TNTs (15 mC cm^{-2}) at 580 nm is 89.71%, which is higher than that of the DSSC with TNT (79.43%), and also IPCE over the whole wavelength region of 400 nm to 800 nm exhibits higher value for the former case, resulting from the more basic surface of Y–TNT for more dye adsorption and therefore more electrons can be excited. All the IPCE values at 580 nm are in consistency with the J_{SC} value of the cells.

Transient photovoltage curves of dye-sensitized solar cells with Y_2O_3 modified TiO_2 nanotube arrays

Transient photovoltage curves were obtained to estimate average electron lifetimes of the DSSCs with TNT and Y–TNT obtained with the charge capacities of 10, 15, 20, and 25 mC cm^{-2}, as shown in **Figure 7**. The average electron lifetimes could approximately be estimated by fitting a decay of the open circuit potential transient with exp ($-t\ \tau_e^{-1}$), where t is time and τ_e is an average time constant before recombination. The τ_e values of 13.18, 24.41, 30.65, 38.77, and 46.69 ms are obtained for the photoanodes with TNT and Y–TNT obtained with the charge capacities of 10, 15, 20, and 25 mC cm^{-2}, respectively. The longer electron life time for the Y–TNT based DSSCs is due to the Y_2O_3 barrier layer to inhibit back transfer of electrons from TiO_2 to triiodide ions. Also, the increasing electron life time for the photoanode with thicker Y_2O_3 barrier layer again confirms that the charge recombination dynamics can be easily controlled by varying the charge capacity for electrodepositing $Y(OH)_3$ and be reduced with more amount of Y_2O_3 on TNT surface. The longer electron life times are in consistency with the higher *V*oc value of the corresponding cells.

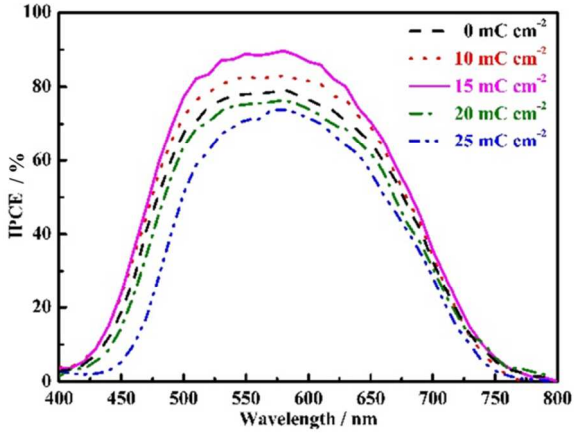

Figure 6 IPCE curves of the DSSCs with bare TNT and Y–TNT obtained with the charge capacities of 10, 15, 20, and 25 mC cm^{-2}.

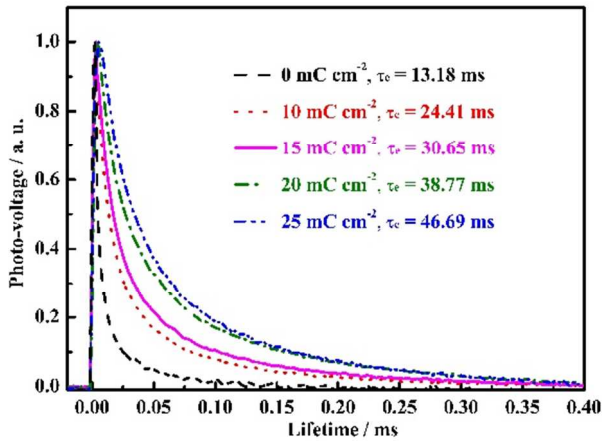

Figure 7 Transient photovoltage curves of the DSSCs with bare TNT and Y–TNTs, in which the Y–TNTs were obtained with the charge capacities of 10, 15, 20, and 25 mC cm^{-2}.

Conclusions

TNT obtained on Ti foils exhibits a nearly constant diameter and increasing length for longer anodization periods. The V_{OC} value decreases while the J_{SC} value increases for the DSSC with longer anodization period to obtain TNT on the photoanode, due to the increasing longer electron diffusion path and larger surface area, but the J_{SC} value decreases for the anodization period reaches 300 min due to the serious recombination. Thin layers of $Y(OH)_3$ were electrodeposited on TNT and subsequently the films were annealed to obtain the Y_2O_3 barrier layers to reduce charge recombination. Higher V_{OC} values were found for the Y–TNT based DSSCs with compared to that of the cell with TNT, demonstrating the reduced recombination for the former cases with the help of Y_2O_3 barrier layers. Also, the V_{OC} value increases considerably with increasing amount of Y_2O_3 on TNT, indicating the charge recombination dynamics can be simply controlled by adjusting the charge capacity for $Y(OH)_3$ electrodeposition. The J_{SC} value increases with increasing charge capacity to deposit $Y(OH)_3$ up to 15 mC cm^{-2}, and decreases with further increases in the charge capacity, due to the more basic surface of Y_2O_3 for more dye adsorption but serious electron transfer inhibition for higher charge capacity. The best η of 6.52% was achieved for the Y–TNT based DSSC with a charge capacity of 15 mC cm^{-2},

while the cell with TNT shows an η of 5.35%. The tendency of V_{OC} is in consistency with the dark current and the electron lifetime, while IPCE values shows the same trend with the J_{SC} value for all the cells

Notes and references

[a]*Department of Chemical Engineering, National Taiwan University, Taipei 10617, Taiwan*
[b]*Department of Chemistry, National Central University, Jhong–Li 32001, Taiwan*
[c]*Institute of Polymer Science and Engineering, National Taiwan University, Taipei 10617, Taiwan*
**Corresponding author: Tel: +886–3–422–7151 ext. 65903; Fax: +886–3–422–7664; E–mail: t610002@cc.ncu.edu.tw*
***Corresponding author: Tel: +886-2-2366-0739; Fax: +886-2-2362-3040; E-mail: kcho@ntu.edu.tw*

1. B. O'Regan and M. Grätzel, *Nature*, 1991, **353**, 737.
2. S. Hore, C. Vetter, R. Kern, H. Smit and A. Hinsch, *Sol. Energy Mater. Sol. Cells*, 2006, **90**, 1176.
3. L. L. Li, C. Y. Tsai, H. P. Wu, C. C. Chen and E. W. G. Diau, *J. Mater. Chem.*, 2010, **20**, 2753.
4. K. Shankar, J. I. Basham, N. K. Allam, O. K. Varghese, G. K. Mor, X. Feng, M. Paulose, J. A. Seabold, K. S. Choi and C. A. Grimes, *J. Phys. Chem. C*, 2009, **113**, 6327.
5. H. G. Yun, J. H. Park, B. S. Bae and M. G. Kang, *J. Mater. Chem.*, 2011, **21**, 3558.
6. K. Nakayama, T. Kubo and Y. Nishikitani, *Appl. Phys. Express*, 2008, **1**, 112301.
7. H. Xu, X. Tao, D. T. Wang, Y. Z. Zheng and J. F. Chen, *Electrochim. Acta*, 2010, **55**, 2280.
8. L. Y. Lin, M. H. Yeh, C. P. Lee, Y. H. Chen, R. Vittal and K. C. Ho, *Electrochim. Acta*, 2011, **57**, 270.
9. S. Yang, Y. Huang, C. Huang and X. Zhao, *Chem. Mater.*, 2002, **14**, 1500.
10. S. G. Chen, S. Chappel, Y. Diamant and A. Zaban, *Chem. Mater.*, 2001, **13**, 4629.
11. Y. Diamant, S. G. Chen, O. Melamed and A. Zaban, *J. Phys. Chem. B*, 2003, **107**, 1977.
12. Z. S. Wang, C. H. Huang, Y. Y. Huang, Y. J. Hou, P. H. Xie, B. W. Zhang and H. M. Cheng, *Chem. Mater.*, 2001, **13**, 678.
13. T. Taguchi, X. T. Zhang, I. Sutanto, K. I. Tokuhiro, T. N. Rao, H. Watanabe, T. Nakamori, M. Uragam and A. Fujishima, *Chem. Commun.*, 2003, 2480.
14. A. Kay and M. Grätzel, *Chem. Mater.*, 2002, **14**, 2930.
15. E. Palomares, J. N. Clifford, S. A. Haque, T. Lutz and J. R. Durrant, *Chem. Commun.*, 2002, 1464.
16. E. Palomares, J. N. Clifford, S. A. Haque, T. Lutz and J. R. Durrant, *J. Am. Chem. Soc.*, 2003, **125**, 475.
17. J. Bandara, C. M. Divarathne and S. D. Nanayakkara, *Sol. Energy Mater.Sol. Cells*, 2004, **81**, 429.
18. P. K. M. Bandaranayake, P. V. V. Jayaweera and K. Tennakone, *Sol. Energy Mater.Sol. Cells*, 2003, **76**, 57.
19. S. A. Haque, E. Palomares, H. M. Upadhyaya, L. Otley, R. J. Potter, A. B. Holmes and J. R. Durrant, *Chem. Commun.*, 2003, 3008.
20. E. Guillén, E. Azaceta, A. Vega Poot, J. Idígoras, J. Echeberría, J. A. Anta and R. Tena Zaera, *J. Phys. Chem. C*, 2013, **117**, 13365.
21. C. Gao, X. Li, B. Lu, L. Chen, Y. Wang, F. Teng, J. Wang, Z. Zhang, X. Pan and E. Xie, *Nanoscale*, 2012, **4**, 3475.
22. J. G. Chen, C. Y. Chen, C. G. Wu, C. Y. Lin, Y. H. Lai, C. C. Wang, H. W. Chen, R. Vittal and K. C. Ho, *J. Mater. Chem.*, 2010, **20**, 7201.
23. S. H. A. Lee, Y. Zhao, E. A. H. Pagan, L. Blasdel, W. J. Youngblood and T. E. Mallouk, *Faraday Discuss.*, 2012, **155**, 165.
24. C. H. Liu, P. C. Juan, C. P. Cheng, G. T. Lai, H. Lee, Y. K. Chen, Y. W. Liu and C. W. Hsu, in Nanoelectronics Conference (INEC), 2010 3rd International, 2010, pp. 1256
25. R. Ivanic, V. Breternitz, V. Tvarozek, I. Novotny, C. Knedlik and V. Rehacek, *J. Electr. Eng.*, 2003, **54**, 83.
26. V. Ioannou-Sougleridis, V. Constantoudis, M. Alexe, R. Scholz, G. Vellianitis and A. Dimoulas, *Thin Solid Films*, 2004, **468**, 303.
27. Z. B. Xie, S. Adams, D. J. Blackwood and J. Wang, *Nanotechnology*, 2008, **19**, 405701.
28. C. C. Chen, H. W. Chung, C. H. Chen, H. P. Lu, C. M. Lan, S. F. Chen, L. Luo, C. S. Hong and E. W. G. Diau, *J. Phys. Chem. C*, 2008, **112**, 19151.
29. C. Y. Chen, M. Wang, J. Y. Li, N. Pootrakulchote, L. Alibabaei, C. H. Ngoc Le, J. D. Decoppet, J. H. Tsai, C. Grätzel, C. G. Wu, S. M. Zakeeruddin and M. Grätzel, *ACS Nano*, 2009, **3**, 3103.
30. L. Y. Lin, C. P. Lee, R. Vittal and K. C. Ho, *J. Power Sources*, 2010, **195**, 4344.
31. L. Han, N. Koide, Y. Chiba, A. Islam and T. Mitate, *C. R. Chim.*, 2006, **9**, 645.
32. L. Han, N. Koide, Y. Chiba and T. Mitate, *Appl. Phys. Lett.*, 2004, **84**, 2433.
33. L. Xie, G. Yin, D. Yan, X. Liao, Z. Huang, Y. Yao, Y. Kang and Y. Liu, *J. Mater. Sci. Mater. Med.*, 2009, **21**, 259.
34. J. M. Wu, *J. Cryst. Growth*, 2004, **269**, 347.
35. J.F. Moulder, W.F. Stickle, P.E. Sobol and K. D. Bomben, *Handbook of X-Ray Photoelectron Spectroscopy: A Reference Book of Standard Spectra for Identification and Interpretation of XPS Data*, Perkin-Elmer Corporation, Physical Electronics Division, 1992.
36. J. Zhang, R. He and X. Liu, *Nanotechnology*, 2013, **24**, 505401.
37. J. Robertson, *J. Vac. Sci. Technol. B*, 2000, **18**, 1785.
38. C. G. V. d. Walle and J. Neugebauer, *Nature*, 2003, **423**, 626.
39. B. Tuttle, *Phys. Rev. B*, 2003, **67**, 155324.

Table of content

Surface Modification of TiO_2 Nanotube Arrays with Y_2O_3 Barrier Layer: Controlling Charge Recombination Dynamics in Dye-sensitized Solar Cells

Lu–Yin Lin[a,b], Min–Hsin Yeh[a], Chia–Yuan Chen,[b] R. Vittal,[a] Chun–Guey Wu[b*] and Kuo–Chuan Ho[a,c**]

[a] *Department of Chemical Engineering, National Taiwan University, Taipei 10617, Taiwan*

[b] *Department of Chemistry, National Central University, Jhong–Li 32001, Taiwan*

[c] *Institute of Polymer Science and Engineering, National Taiwan University, Taipei 10617, Taiwan*

**Corresponding author: Tel: +886–3–422–7151 ext. 65903; Fax: +886–3–422–7664;*

E–mail: t610002@cc.ncu.edu.tw

***Corresponding author: Tel: +886-2-2366-0739; Fax: +886-2-2362-3040; E-mail: kcho@ntu.edu.tw*